Biologic Correlates of Intratumoral Heterogeneity in ^{18}F-FDG Distribution with Regional Expression of Glucose Transporters and Hexokinase-II in Experimental Tumor

Songji Zhao, MD[1,2]; Yuji Kuge, PhD[2]; Takafumi Mochizuki, MD[3]; Toshiyuki Takahashi, MD[4]; Kunihiro Nakada, MD[1]; Masayuki Sato, BS[1]; Toshiki Takei, MD[1]; and Nagara Tamaki, MD[1]

[1]Department of Nuclear Medicine, Graduate School of Medicine, Hokkaido University, Sapporo, Japan; [2]Department of Tracer Kinetics, Graduate School of Medicine, Hokkaido University, Sapporo, Japan; [3]Department of Radiology, Nikko Memorial Hospital, Muroran, Japan; and [4]Department of Pathology, Hokkaido Gastroenterology Hospital, Sapporo, Japan

The biologic mechanisms involved in the intratumoral heterogeneous distribution of ^{18}F-FDG have not been fully investigated. To clarify factors inducing heterogeneous ^{18}F-FDG distribution, we determined the intratumoral distribution of ^{18}F-FDG by autoradiography (ARG) and compared it with the regional expression levels of glucose transporters Glut-1 and Glut-3 and hexokinase-II (HK-II) in a rat model of malignant tumor. **Methods:** Rats were inoculated with allogenic hepatoma cells (KDH-8) into the left calf muscle ($n = 7$). Tumor tissues were excised 1 h after the intravenous injection of ^{18}F-FDG and sectioned to obtain 2 adjacent slices for ARG and histochemical studies. The regions of interest (ROIs) were placed on ARG images to cover mainly the central (CT) and peripheral (PT) regions of viable tumor tissues and necrotic/apoptotic (NA) regions. The radioactivity in each ROI was analyzed quantitatively using a computerized imaging analysis system. The expression levels of Glut-1, Glut-3, and HK-II were determined by immunostaining and semiquantitative evaluation. The hypoxia-inducible factor 1α (HIF-1α) was also immunostained. **Results:** ARG images showed that intratumoral ^{18}F-FDG distribution was heterogeneous. The accumulation of ^{18}F-FDG in the CT region was the highest, which was 1.6 and 2.3 times higher than those in the PT and NA regions, respectively ($P < 0.001$). The expression levels of Glut-1, Glut-3, and HK-II were markedly higher in the CT region ($P < 0.001$) compared with those in the PT region. The intratumoral distribution of ^{18}F-FDG significantly correlated with the expression levels of Glut-1, Glut-3, and HK-II ($r = 0.923$, $P < 0.001$ for Glut-1; $r = 0.829$, $P < 0.001$ for Glut-3; and $r = 0.764$, $P < 0.01$ for HK-II). The positive staining of HIF-1α was observed in the CT region. **Conclusion:** These results demonstrate that intratumoral ^{18}F-FDG distribution corresponds well to the expression levels of Glut-1, Glut-3, and HK-II. The elevated expression levels of Glut-1, Glut-3, and HK-II, induced by hypoxia (HIF-1α), may be contributing factors to the higher ^{18}F-FDG accumulation in the CT region.

Key Words: ^{18}F-FDG; glucose transporters; hexokinase; heterogeneity; tumor

J Nucl Med 2005; 46:675–682

PET using ^{18}F-FDG has been widely used not only for detecting and staging malignant tumors but also for monitoring therapy response and for differentiating malignant lesions from benign lesions (*1–4*). These applications are based on the increased ^{18}F-FDG uptake due to enhanced glucose utilization in most tumors. The increased ^{18}F-FDG accumulation in malignant tumors is associated with the rate of transport across the cell membrane, the activity of hexokinase, and the rate of dephosphorylation in the tissue (*5,6*). The transport of ^{18}F-FDG across cell membranes is mediated by ≥5 structurally related proteins (constituting a family of glucose transporters, Glut-1 to Glut-5) (*7,8*). Significantly elevated expression levels of Glut-1 and Glut-3 are considered to be a factor contributing to the accumulation of ^{18}F-FDG in malignant tumors (*9–13*). It has also been suggested that the activity level of hexokinase-II (HK-II) contributes to ^{18}F-FDG accumulation in various malignant tumors (*14*). These studies, however, used PET or tissue-counting techniques and correlated average ^{18}F-FDG accumulation in the tumor with protein expression.

It is well known that various components, including nonmalignant components, are involved in most solid tumors (*15–17*). Tumor tissues also show intratumoral heterogeneity in their various properties, which may originate from the diverse phenotypic properties of tumor cells or may be induced by their metabolic microenvironment (*18–20*). In this regard, intratumoral heterogeneity in ^{18}F-FDG distribution has been well demonstrated by autoradiography (ARG)

Received Sep. 3, 2004; revision accepted Nov. 23, 2004.

For correspondence or reprints contact: Nagara Tamaki, MD, Department of Nuclear Medicine, Graduate School of Medicine, Hokkaido University, Kita 15 Nishi 7, Kita-ku, Sapporo 060-8638, Japan.

E-mail: natamaki@med.hokudai.ac.jp

(*15*). However, there have been few reports regarding the biologic mechanisms involved in the intratumoral heterogeneous distribution of ^{18}F-FDG. The relationships between the intratumoral distribution of ^{18}F-FDG and the regional expression of glucose transporters or hexokinases remain to be investigated. Such data should be helpful in understanding the mechanism of ^{18}F-FDG uptake in malignant tumors and should provide the biologic basis for diagnosing, staging, and prognosticating malignant tumors and monitoring therapy response by ^{18}F-FDG PET.

To clarify factors inducing heterogeneous ^{18}F-FDG distribution, we determined in this study the intratumoral distribution of ^{18}F-FDG by ARG and compared it with the regional expression levels of Glut-1, Glut-3, and HK-II in a rat model of malignant tumor.

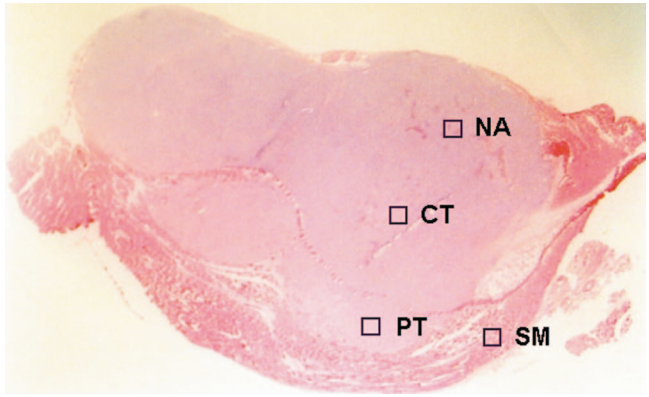

FIGURE 1. ROIs were placed on ARG image, to cover mainly central (CT) and peripheral (PT) regions of viable tumor tissues and necrotic/apoptotic (NA) regions, with reference to corresponding sections stained with HE. SM = surrounding muscle.

MATERIALS AND METHODS

Animal Studies

The experimental protocol was completely approved by the Laboratory Animal Care and Use Committee of Hokkaido University. Male Wistar King Aptekman/hok (WKAH) rats, weighing 203–268 g, were inoculated with a suspension of allogenic hepatoma cells (KDH-8, 1×10^6 cells per rat) into the left calf muscle. Two weeks after the tumor inoculation, when the tumors were 2–3 cm in diameter, the rats were fasted overnight ($n = 7$) (*21*). Each rat was anesthetized with pentobarbital (50 mg/kg body weight, intraperitoneally) and was injected in the tail vein with 37 MBq of ^{18}F-FDG synthesized as previously described (*22*). Sixty minutes after the ^{18}F-FDG injection, the animals were sacrificed and the tumors were quickly excised. Each tumor tissue was then sectioned at 2- to 3-mm thickness to obtain 2 adjacent slices. One of the 2 slices was embedded in Tissue-Tek medium (Sakura Finetechnical Co., Ltd.) and frozen in isopentane/dry ice for ARG studies. Formalin-fixed, paraffin-embedded specimens were prepared using the other slice for subsequent histochemical studies (*23*).

ARG Studies

The frozen samples were cut into 20-μm sections with a CM3050-Cryostat (Leica) at −20°C. The tumor sections were placed in a phosphor image plate cassette, together with a set of calibrated standards (*17*), and an overnight ARG exposure was used to detect the distribution of ^{18}F-FDG. The tumor sections (10 μm) adjacent to those used for the ARG studies were stained with hematoxylin and eosin (HE) for use as the reference to determine the regions of interest (ROIs) on the autoradiograms.

The ARG images were analyzed using a computerized imaging analysis system (BAS 5000 Bio-Imaging Analyzer; Fuji Photo Film Co., Ltd.). The resolution of ARG of the BAS 5000 is 100 μm. To quantitatively evaluate the distribution of ^{18}F-FDG radioactivity, 32 ROIs (0.36 mm^2) were determined on each ARG image. ROIs were placed to cover mainly the central (CT; $n = 8$) and peripheral (PT; $n = 8$) regions of the viable tumor tissues, necrotic/apoptotic (NA; $n = 8$) regions, and the surrounding muscle (SM; $n = 8$), by referring to the sections stained with HE (Fig. 1); each ROI was selected microscopically by a pathologist and identified by its predominant histologic characteristic as a region of the viable tumor cells and necrotic/apoptotic cells in the CT and PT regions on the HE section. Large necrotic regions occasionally observed in the center of the tumors were excluded from the evaluation. To avoid any bias, these ROIs were determined in a blind manner for ARG images and immunologic staining (Gluts and HK-II). The ROIs placed on HE images were transferred to ARG images by using computer software (MCID-M2 Image Analyzer; Imaging Research Inc.). Briefly, coordinates were set on both HE and ARG images, the coordinates of each ROI on the HE images was determined, and then each ROI was transferred to the same coordinates of the corresponding ARG images. The radioactivity in each ROI was shown by photostimulated luminescence per unit area, PSL/mm^2 ($PSL = a \cdot D \cdot t$: a = constant; D = radioactivity exposed on imaging plate; t = exposed time); then each count of PSL/mm^2 from a tumor section was recorded and used to calculate the mean counts per mm^2 and converted to the percentage injected dose per gram (%ID/g) of tissue by using activity of the standards, with the assumption that tissue density is 1 g/cm^3 (*17,24*). The mean radioactivities of the 8 ROIs determined for the CT, PT, NA regions, and SM, respectively, were used to evaluate the ^{18}F-FDG accumulation in the tissues.

Histochemical Studies

The expression of Glut-1, Glut-3, and HK-II was studied in the sections of a formalin-fixed, paraffin-embedded tumor according to a standard immunostaining procedure (*10,25*). Briefly, after deparaffization and rehydration, endogenous peroxidase activity was blocked for 10 min in methanol containing 3% hydrogen peroxide. Thereafter, endogenous nonspecific antigens were blocked in 10% normal goat albumin (HISTOFINE SAB-PO kit; Nichirei) for 10 min at 37°C and then incubated with an anti-Glut-1, anti-Glut-3, or antihexokinase II antibody (Chemicon International Inc.) for 30 min at 37°C. The bound antibody was visualized using the avidin/biotin conjugate immunoperoxidase procedure (ABC) with the HISTOFINE SAB-PO kit and 3,3′-diaminobenzidine tetrahydrochloride. Tumor sections adjacent to those used for these histochemical studies were also stained with anti-HIF-1α (mouse antihypoxia-inducible factor 1α monoclonal IgG 2b, clone H1α67; Novus Biologicals) using the method of Zhong et al. (*26*) with slight modification. Briefly, after deparaffinization and rehydration, the slides were initially immersed in a target retrieval solution (10 mmol/L ethylenediaminetetraacetic acid, pH 8.0) and heated in a microwave oven (500 W) for 20 min.

After the antigen retrieval, endogenous peroxidase activity was blocked for 5 min in methanol containing 3% hydrogen peroxide. Thereafter, endogenous nonspecific antigens were blocked in 10% hog albumin (Cosmo Bio., Ltd.) for 10 min and then incubated overnight with the primary antibody at 4°C. Finally, the bound antibody was visualized using the ABC procedure with the HISTOFINE MAX-PO (M) kit (Nichirei) and 3,3′-diaminobenzidine tetrahydrochloride. Tumor sections adjacent to those used for the immunostaining were stained with HE.

For immunohistochemical grading, ROIs placed on the HE-stained sections were transferred to immunologically stained sections as described. The intensity of staining and the percentage of positively stained cells in the CT ($n = 8$) and PT ($n = 8$) regions of the viable tumor tissues were evaluated microscopically. The intensity of staining (intensity) was graded from 0 to 3 (0 = not stained, 1 = equivocal, 2 = intense, and 3 = very intense) according to the criteria of Higashi et al. (*27*). Moreover, the percentage of positively stained cells (% positive) was classified from 1 to 5 (1 = 0%–20%, 2 = 20%–40%, 3 = 40%–60%, 4 = 60%–80%, and 5 = 80%–100%). The expression levels of Gluts and HK-II were assessed semiquantitatively using the product of these scores (intensity × % positive) (*28*). In HIF-1α staining, cells with completely and darkly stained nuclei were regarded as positively stained cells (*29*).

Statistical Analysis

All values are expressed as mean ± SD. One-way ANOVA and the Bonferroni post hoc test were used to assess the significance of differences due to the intratumoral distribution of ^{18}F-FDG. To evaluate the significance of differences in the expression levels of Glut-1, Glut-3, and HK-II (intensity × % positive) between the CT and PT regions, an unpaired Student *t* test was performed. Simple regression analysis was used to compare the intratumoral ^{18}F-FDG distribution and the expression levels of Glut-1, Glut-3, and HK-II. A 2-tailed P value < 0.05 was considered significant.

RESULTS

Intratumoral Distribution of ^{18}F-FDG

Figure 2A shows the representative autoradiogram of ^{18}F-FDG distribution in the tumor. The ARG images showed heterogeneous ^{18}F-FDG distribution with a relatively higher ^{18}F-FDG accumulation level in the CT regions of viable tumor tissues.

Results from the quantitative evaluation of ^{18}F-FDG distribution are summarized in Figure 2B. The accumulation of ^{18}F-FDG in the CT region was the highest (4.43 ± 0.50 %ID/g), which was 1.6 and 2.3 times higher than those in the PT region (2.85 ± 0.22 %ID/g) and the NA region (1.94 ± 0.10 %ID/g), respectively ($P <$ 0.001). The accumulation of ^{18}F-FDG in the PT region was 1.5 times and was significantly higher than that in the NA region ($P < 0.001$). The distribution of ^{18}F-FDG in the SM (0.18 ± 0.01 %ID/g) was lower than those in any other ROIs determined in the tumor tissues (CT, PT, and NA).

Immunohistochemical Staining

The typical immunostaining of Glut-1, Glut-3, and HK-II in the CT and PT region is shown in Figure 3. The intensity and extent of staining of Glut-1, Glut-3, and HK-II were markedly higher in the CT region than those in the PT region.

The results of immunohistochemical grading are summarized in Figure 4. The histochemical grading scores for Glut-1 and Glut-3 were significantly higher in the CT region (11.34 ± 1.78 for Glut-1 and 6.02 ± 1.83 for Glut-3) than those in the PT region (4.23 ± 0.85 for Glut-1 and 2.29 ± 0.62 for Glut-3; $P < 0.001$ for both). The histochemical grading score for HK-II was also significantly higher in the

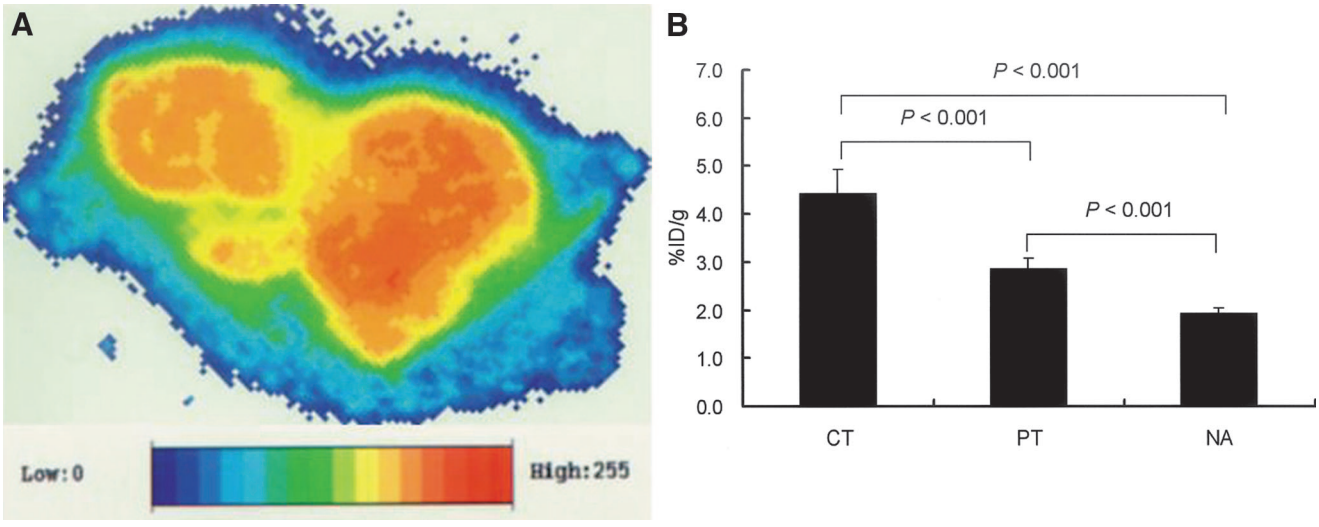

FIGURE 2. (A) Representative autoradiograph of ^{18}F-FDG distribution. ARG image shows intratumoral heterogeneous ^{18}F-FDG distribution. (B) Quantitative evaluation of intratumoral ^{18}F-FDG distribution. ^{18}F-FDG accumulation level in CT region was highest, which was 1.6 and 2.3 times higher than those in PT and NA regions, respectively ($P < 0.001$).

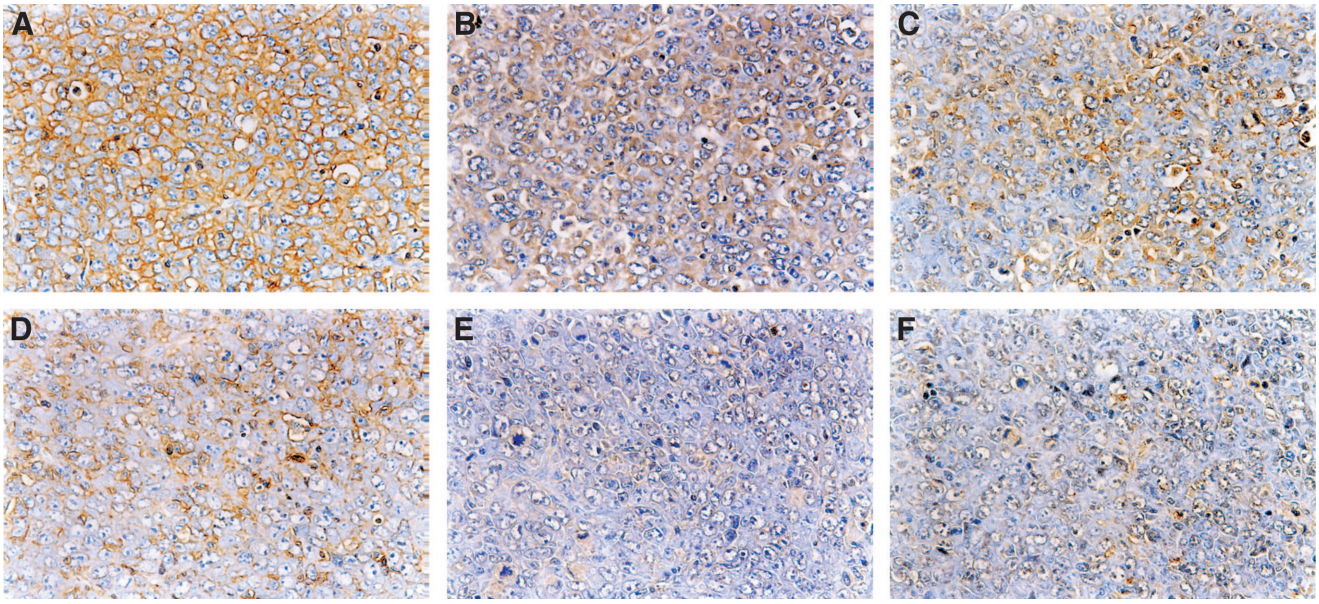

FIGURE 3. Staining with anti-Glut-1 (A and D), anti-Glut-3 (B and E), and anti-HK-II (C and F) antibodies in CT region (top) was more prominent than those in PT region (bottom) in KDH-8 tumor tissues, respectively (×400).

CT region (4.25 ± 0.98) compared with that in the PT region (2.00 ± 0.28; $P < 0.001$). The positive staining of HIF-1α was clearly observed in the CT region (Fig. 5) but not in the PT region.

Relationships Between ^{18}F-FDG Accumulation and Expression Levels of Gluts and HK-II

The accumulation of ^{18}F-FDG and the expression levels of Glut-1, Glut-3, and HK-II were significantly higher in the CT region than those in the PT region (Figs. 2 and 4). Figure 6 shows scattergrams of histochemical grading scores and ^{18}F-FDG accumulation. Intratumoral ^{18}F-FDG accumulation significantly correlated with the expression levels of Glut-1, Glut-3, and HK-II: $r = 0.923$, $P < 0.001$ for Glut-1; $r = 0.829$, $P < 0.001$ for Glut-3; and $r = 0.764$, $P < 0.01$ for HK-II.

DISCUSSION

In this study, a relatively higher ^{18}F-FDG accumulation was observed in the CT regions, with elevated expression levels of Glut-1, Glut-3, and HK-II. Positive staining of HIF-1α was observed in these regions. Intratumoral ^{18}F-FDG distribution significantly correlated with the expression levels of Glut-1, Glut-3, and HK-II. Consequently, the regional expression levels of Glut-1, Glut-3, and HK-II may increase in a hypoxic environment within tumor tissues and may contribute to heterogeneous ^{18}F-FDG distribution in the tumor tissues.

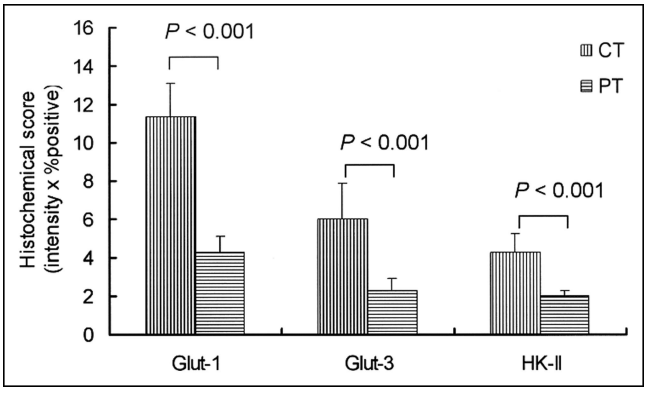

FIGURE 4. Expression levels of Glut-1, Glut-3, and HK-II were assessed by semiquantitative immunohistochemical grading performed by calculating the product of these scores (intensity × % positive). Histochemical scores of Glut-1, Glut-3, and HK-II were significantly higher in CT region than those in PT region ($P < 0.001$).

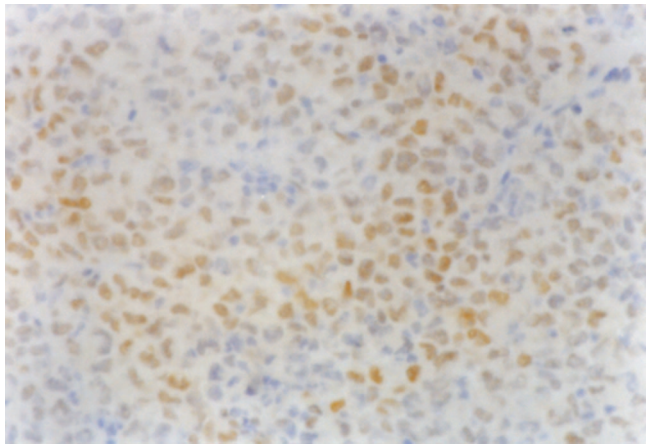

FIGURE 5. Positive staining of HIF-1α was clearly observed in CT region (×400).

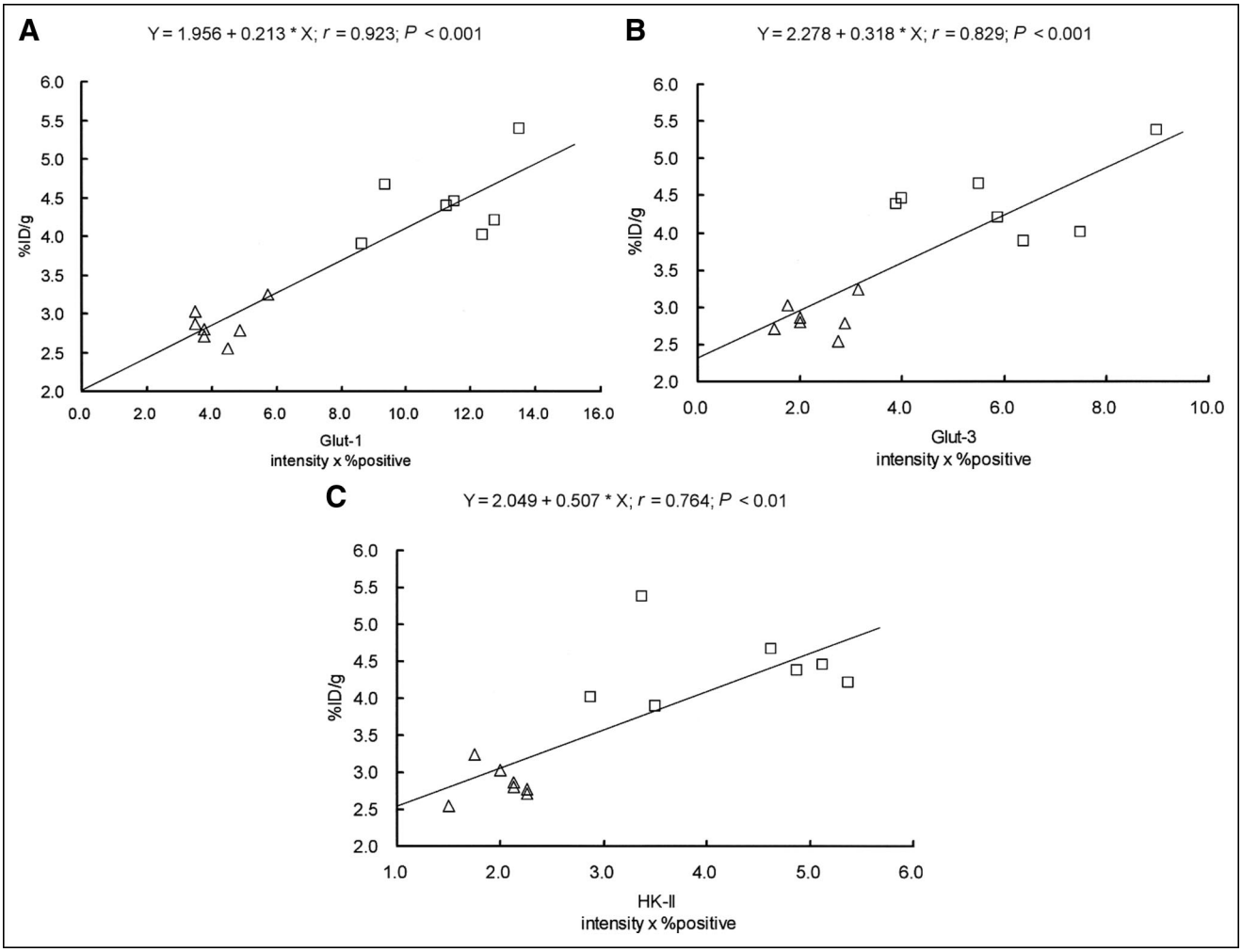

FIGURE 6. Relationships between expression levels of Glut-1, Glut-3, and HK-II and intratumoral ^{18}F-FDG accumulation in KDH-8 tumor tissues. Intratumoral ^{18}F-FDG accumulation significantly correlated with expression levels of Glut-1, Glut-3, and HK-II (intensity × % positive). (A) Relationship between ^{18}F-FDG accumulation and histochemical grading score for Glut-1. (B) Relationship between ^{18}F-FDG accumulation and histochemical grading score for Glut-3. (C) Relationship between ^{18}F-FDG accumulation and histochemical grading score for HK-II. □, CT region; △, PT region.

Although intratumoral heterogeneity in ^{18}F-FDG distribution has been demonstrated (*15*), there have been few reports with regard to the biologic mechanisms involved in the intratumoral heterogeneous distribution of ^{18}F-FDG. The present results showed a significant correlation between the intratumoral distribution of ^{18}F-FDG and the regional expression level of Glut-1, which is consistent with the results of syngeneic rat mammary cancer reported by Brown et al. (*30*). In addition, our results demonstrated—to our knowledge, for the first time—that intratumoral ^{18}F-FDG distribution significantly correlates with the regional expression levels of Glut-3 and HK-II. The heterogeneity in ^{18}F-FDG distribution may be ascribed to the altered expression levels of Glut-1, Glut-3, and HK-II and may reflect a metabolic microenvironment of tumors.

Aggressive tumors often have insufficient blood supply. Hypoxia occurs in tissue that is >100–200 μm away from a functional blood supply. When the tumors are exposed to a hypoxic environment, HIF-1α is activated to promote the transcription of several genes, including glucose transporters and glycolytic enzymes (*31*). The increased uptake of ^{3}H-FDG in vitro by hypoxic tumor cells has been well demonstrated (*32*). Recently, Dearling et al. (*33*) have extended the previous in vitro work and confirmed the selectivity of ^{18}F-FDG for hypoxic regions over normoxic regions in vivo. In the present study, a relatively higher ^{18}F-FDG accumulation was observed in the CT region, with elevated expression levels of Glut-1, Glut-3, and HK-II. The positive staining of HIF-1α was observed in these regions. Taken altogether, the regional expression levels of Glut-1, Glut-3, and HK-II may be increased by HIF-1α in a hypoxic environment within the tumor tissue and may contribute to the elevated ^{18}F-FDG accumulation.

Several studies have focused on the expression of Gluts and hexokinase activity to define the role of these proteins in the regulation of ^{18}F-FDG accumulation (*34,35*). Elevated expression levels of Glut-1 and Glut-3 are considered to be factors that contribute to the accumulation of ^{18}F-FDG in malignant tumors (*9–13,23,28*). It has also been suggested that the activity level of HK-II contributes to ^{18}F-FDG accumulation in various malignant tumors (*14*). Chromatographic, polyclonal antibody, and amino acid analyses indicated that rat hepatoma hexokinase is most closely related to HK-II and suggests that mitochondrial hexokinase activity determines the rate of accumulation of ^{18}F-FDG in tumors (*36*). These studies, however, used PET or tissue-counting techniques and correlated average ^{18}F-FDG accumulation in the tumor with protein expression. The biologic mechanisms involved in intratumoral heterogeneity in ^{18}F-FDG distribution have not been fully investigated. The present results demonstrate that the expression levels of Glut-1, Glut-3, and HK-II also contribute to intratumoral heterogeneity in ^{18}F-FDG distribution in our model rats, as determined using an ARG technique. It is crucial to consider the relative contributions of Glut-1, Glut-3, and HK-II to intratumoral ^{18}F-FDG accumulation. Unfortunately, we could not determine the relative contributions of these proteins, mainly due to the limited number of samples used in this study. Further studies are required to clarify the respective contributions of glucose transporters and hexokinase to intratumoral heterogeneity in ^{18}F-FDG accumulation.

Intratumoral ^{18}F-FDG distribution has been described at the cellular level by several investigators (*15–20*). Kubota et al. showed that ^{18}F-FDG preferentially accumulates in macrophages and young granulation tissues surrounding necrotic foci rather than in tumor cells using a malignant tumor mouse model (*15*). In contrast, Brown et al. (*17*) observed relatively less ^{3}H-FDG accumulation in necrotic/inflammatory infiltration compared with that in the tumor cells. Our results in rats confirmed intratumoral heterogeneity in ^{18}F-FDG distribution. The ^{18}F-FDG accumulation in the CT regions was 1.6 and 2.3 times higher than those in the PT and NA regions, respectively. Our results are consistent with the results reported by Brown et al.

In this study, the regions of viable tumor tissues and NA regions in ARG were identified using the HE-stained sections as reference. Apoptosis was most reliably assayed by morphologic counts using HE staining. Since there are some apoptotic cancer cells interwoven in necrotic regions and it was difficult to clearly distinguish apoptotic cells from necrotic cells in the present study, the term NA regions is used. Viable tumor cells and necrotic/apoptotic cells were also interwoven; thus, we used relatively small ROIs to clearly divide the regions between the viable tumor cells and necrotic/apoptotic cells. The larger ROIs appeared to cover both of the viable tumor cells and necrotic/apoptotic cells. Brown et al. (*17*) also used such ROI analysis to evaluate intratumoral distribution of ^{18}F-FDG. On the other hand, because necrotic cells revealed cell injuries in morphology—such as the cell membrane appearing ruptured, the nuclear chromatin being markedly condensed or pyknotic, vesicular structures filling the cytoplasm, and fusion of organelles (*37*)—the immunohistochemical staining of Glut-1, Glut-3, and HK-II cannot reflect the antigenicity of cells. Therefore, the expression levels of Glut-1, Glut-3, and HK-II were not investigated by immunostaining and semiquantitative evaluation in the NA regions. The slices immunohistochemically stained for Glut-1, Glut-3, and HK-II were from the formalin-fixed, paraffin-embedded specimens, but those used in ARG imaging to determine regional ^{18}F-FDG distribution were from the frozen samples. Thus, selected areas in the immunohistochemical staining for Glut-1, Glut-3, and HK-II of the CT, PT, and NA regions were not exactly congruent with those for determining regional ^{18}F-FDG distribution on ARG imaging, although both formalin-fixed, paraffin-embedded specimens and frozen samples were adjacent. It is important to note that expression of Glut-1, Glut-3, and hexokinase II (as determined in this study) does not generally imply increased functional activity. Several studies have demonstrated that hexokinase bound to the mitochondrial membrane has a much higher catalytic activity than cytosolic hexokinase. Aloj et al. (*14*) have also indicated that ^{18}F-FDG uptake correlates better with ^{18}F-FDG phosphorylating activity of mitochondrial preparations than with the level of expression of the Glut-1 or hexokinase I or II genes. The excellent correlation between HK-II expression and ^{18}F-FDG uptake observed in the present study may not be representative for other tumor models.

In our study, ARG imaging was performed 1 h after ^{18}F-FDG injection. The 1-h time point is widely used also in rodent models, and no significant differences in the ^{18}F-FDG uptake were observed in the mouse tumor tissues between 1 and 2 h after ^{18}F-FDG injection (*33*). However, further studies at more than one time point are needed to give an indication of the time course of ^{18}F-FDG uptake and to compare with the present results in rodent-bearing xenografts.

^{18}F-FDG PET has become increasingly important not only for detecting and staging malignant tumors but also for monitoring therapy response and for differentiating malignant lesions from benign lesions (*1–4*). However, variable tumor accumulation of ^{18}F-FDG has been indicated to prevent accurate diagnosis by ^{18}F-FDG PET (*38,39*). Intratumoral heterogeneity in ^{18}F-FDG distribution may also affect such diagnostic accuracy. The present study provides a biologic basis of intratumoral heterogeneity in ^{18}F-FDG distribution, which leads to better understanding of the mechanism of ^{18}F-FDG accumulation in tumors and contributes to the accurate diagnosis of patients with malignant tumors by ^{18}F-FDG PET. On the other hand, recent advances in radiation therapy such as intensity-modulated radiation therapy have exploited new areas for the use of

^{18}F-FDG PET (*40*). Regions of high ^{18}F-FDG uptake can be treated with a higher radiation dose compared with a hypometabolic portion of the same mass. In addition, glucose transporters (Glut-1 and Glut-3) and glycolytic enzymes (for example, hexokinase) are promoted by activated HIF-1α (*31*). The present study showed an excellent correlation between regional ^{18}F-FDG uptake and the expression of facilitative glucose transporters (Glut-1 and Glut-3) and HK-II. Furthermore, this study found that ^{18}F-FDG uptake was more intense in tumor regions that express HIF-1α. Recent clinical data indicate that hypoxic tumors are known to be more malignant, to be more likely to metastasize, and to have a poor prognosis. HIF-1α is considered to be a key factor for tumor progression by upregulating genes involved in angiogenesis, cell survival, cell invasion, and resistance to drug therapy and radiotherapy. Thus, the findings of this study suggest that tumor areas with high ^{18}F-FDG uptake may represent biologically more aggressive cancer cells. This has important consequences for the use of ^{18}F-FDG PET for treatment planning—particularly, intensity-modulated radiation therapy. ^{18}F-FDG PET could help to identify regions for dose-escalation protocols. We believe that our data also provide useful information in a precision radiation therapy protocol with modern radiotherapy modalities.

CONCLUSION

The colocalization of a high ^{18}F-FDG level and Glut-1, Glut-3, and HK-II overexpression in regions that are likely to be subjected to hypoxia as well as the strong correlation between the transporters and HK-II expression and ^{18}F-FDG accumulation suggest that enhanced transmembrane transport and phosphorylation may be part of an adaptive mechanism triggered by changes in the metabolic microenvironment of cancer cells. The regional expression levels of Glut-1, Glut-3, and HK-II may increase in a hypoxic environment within tumor tissues and may contribute to intratumoral heterogeneous ^{18}F-FDG distribution. The present results lead to a better understanding of the mechanism of ^{18}F-FDG accumulation in tumors, which may help in interpreting ^{18}F-FDG accumulation in patients with malignant tumors.

ACKNOWLEDGMENTS

This work was supported in part by a grant-in-aid for Scientific Research from the Japan Society for the Promotion of Science and in part by the Japanese Ministry of Education, Culture, Sports, Science and Technology and by a grant from the Rotary Yoneyama Memorial Foundation, Inc. The authors are grateful to the staff of the Nuclear Medicine and Central Institute of Isotope Science, Hokkaido University, for supporting this work. We also thank Mr. Kenichi Nishijima for technical assistance.

REFERENCES

1. Delbeke D, Rose DM, Chapman WC, et al. Optimal interpretation of FDG PET in the diagnosis, staging and management of pancreatic carcinoma. *J Nucl Med.* 1999;40:1784–1791.
2. Higashi T, Sakahara H, Torizuka T, et al. Evaluation of intraoperative radiation therapy for unresectable pancreatic cancer with FDG PET. *J Nucl Med.* 1999; 40:1424–1433.
3. Schelling M, Avril N, Nahrig J, et al. Positron emission tomography using [^{18}F]fluorodeoxyglucose for monitoring primary chemotherapy in breast cancer. *J Clin Oncol.* 2000;18:1689–1695.
4. Dimitrakopoulou-Strauss A, Strauss LG, Heichel T, et al. The role of quantitative ^{18}F-FDG PET studies for the differentiation of malignant and benign bone lesions. *J Nucl Med.* 2002;43:510–518.
5. Haberkorn U, Ziegler SI, Oberdorfer F, et al. FDG uptake, tumor proliferation and expression of glycolysis associated genes in animal tumor models. *Nucl Med Biol.* 1994;21:827–834.
6. Golshani-Hebroni SG, Bessman SP. Hexokinase binding to mitochondria: a basis for proliferative energy metabolism. *J Bioenerg Biomembr.* 1997;29:331–338.
7. Bell GI, Burant CF, Takeda J, Gould GW. Structure and function of mammalian facilitative sugar transporters. *J Biol Chem.* 1993;268:19161–19164.
8. Brown RS, Leung JY, Kison PV, Zasadny KR, Flint A, Wahl RL. Glucose transporters and FDG uptake in untreated primary human non-small cell lung cancer. *J Nucl Med.* 1999;40:556–565.
9. Reske SN, Grillenberger KG, Glatting G, et al. Overexpression of glucose transporter 1 and increased FDG uptake in pancreatic carcinoma. *J Nucl Med.* 1997;38:1344–1348.
10. Brown RS, Wahl RL. Overexpression of Glut-1 glucose transporter in human breast cancer: an immunohistochemical study. *Cancer.* 1993;72:2979–2985.
11. Boado RJ, Black KL, Pardridge WM. Gene expression of Glut-3 and Glut-1 glucose transporters in human brain tumors. *Brain Res Mol Brain Res.* 1994;27: 51–57.
12. Younes M, Brown RW, Stephenson M, Gondo M, Cagle PT. Overexpression of Glut-1 and Glut-3 in stage I nonsmall cell lung carcinoma is associated with poor survival. *Cancer.* 1997;80:1046–1051.
13. Suzuki T, Iwazaki A, Katagiri H, et al. Enhanced expression of glucose transporter Glut-3 in tumorigenic HeLa cell hybrids associated with tumor suppressor dysfunction. *Eur J Biochem.* 1999;262:534–540.
14. Aloj L, Caracó C, Jagoda E, Eckelman WC, Neumann RD. Glut-1 and hexokinase expression: relationship with 2-fluoro-2-deoxy-D-glucose uptake in A431 and T47D cells in culture. *Cancer Res.* 1999;59:4709–4714.
15. Kubota R, Yamada S, Kubota K, Ishiwata K, Tamahashi N, Ido T. Intratumoral distribution of fluorine-18-fluorodeoxyglucose in vivo: high accumulation in macrophages and granulation tissues studied by microautoradiography. *J Nucl Med.* 1992;33:1972–1980.
16. Kubota R, Kubota K, Yamada S, Tada M, Ido T, Tamahashi N. Microautoradiographic study for the differentiation of intratumoral macrophages, granulation tissues and cancer cells by the dynamics of fluorine-18-fluorodeoxyglucose uptake. *J Nucl Med.* 1994;35:104–112.
17. Brown RS, Leung JY, Fisher SJ, Frey KA, Ethier SP, Wahl RL. Intratumoral distribution of tritiated fluorodeoxyglucose in breast carcinoma. I. Are inflammatory cells important? *J Nucl Med.* 1995;36:1854–1861.
18. Kubota R, Kubota K, Yamada S, Tada M, Ido T, Tamahashi N. Active and passive mechanisms of [fluorine-18]fluorodeoxyglucose uptake by proliferating and prenecrotic cancer cells in vivo: a microautoradiographic study. *J Nucl Med.* 1994;35:1067–1075.
19. Kubota R, Kubota K, Yamada S, et al. Methionine uptake by tumor tissue: a microautoradiographic comparison with FDG. *J Nucl Med.* 1995;36:484–492.
20. Reinhardt MJ, Kubota K, Yamada S, Iwata R, Yaegashi H. Assessment of cancer recurrence in residual tumors after fractionated radiotherapy: a comparison of fluorodeoxyglucose, L-methionine and thymidine. *J Nucl Med.* 1997;38:280–287.
21. Zhao S, Kuge Y, Tsukamoto E, et al. Effects of insulin and glucose loading on FDG uptake in experimental malignant tumours and inflammatory lesions. *Eur J Nucl Med.* 2001;28:730–735.
22. Toorongian SA, Mulholland GK, Jewett DM, Bachelor MA, Kilbourn MR. Routine production of 2-deoxy-2-[^{18}F]fluoro-D-glucose by direct nucleophilic exchange on a quaternary 4-aminopyridinium resin. *Nucl Med Biol.* 1990;17: 273–279.
23. Zhao S, Kuge Y, Tsukamoto E, et al. Fluorodeoxyglucose uptake and glucose transporter expression in experimental inflammatory lesions and malignant tumours: effects of insulin and glucose loading. *Nucl Med Commun.* 2002;23:545–550.

24. Toyama H, Ichise M, Liow JS, et al. Absolute quantification of regional cerebral glucose utilization in mice by ^{18}F-FDG small animal PET scanning and 2-^{14}C-DG autoradiography. *J Nucl Med.* 2004;45:1398–1405.
25. Higashi T, Saga T, Nakamoto Y, et al. Relationship between retention index in dual-phase ^{18}F-FDG PET, and hexokinase-II and glucose transporter-1 expression in pancreatic cancer. *J Nucl Med.* 2002;43:173–180.
26. Zhong H, De Marzo AM, Laughner E, et al. Overexpression of hypoxia-inducible factor 1α in common human cancers and their metastases. *Cancer Res.* 1999;59: 5830–5835.
27. Higashi T, Tamaki N, Honda T, et al. Expression of glucose transporters in human pancreatic tumors compared with increased FDG accumulation in PET study. *J Nucl Med.* 1997;38:1337–1344.
28. Mochizuki T, Tsukamoto E, Kuge Y, et al. FDG uptake and glucose transporter subtype expressions in experimental tumor and inflammation models. *J Nucl Med.* 2001;42:1551–1555.
29. Bos R, Zhong H, Hanrahan CF, et al. Levels of hypoxia-inducible factor-1α during breast carcinogenesis. *J Natl Cancer Inst.* 2001;93:309–314.
30. Brown RS, Leung JY, Fisher SJ, Frey KA, Ethier SP, Wahl RL. Intratumoral distribution of tritiated-FDG in breast carcinoma: correlation between Glut-1 expression and FDG uptake. *J Nucl Med.* 1996;37:1042–1047.
31. Dang CV, Semenza GL. Oncogenic alterations of metabolism. *Trends Biochem Sci.* 1999;24:68–72.
32. Clavo AC, Brown RS, Wahl RL. Fluorodeoxyglucose uptake in human cancer cell lines is increased by hypoxia. *J Nucl Med.* 1995;36:1625–1632.
33. Dearling JL, Flynn AA, Sutcliffe-Goulden J, et al. Analysis of the regional uptake of radiolabeled deoxyglucose analogs in human tumor xenografts. *J Nucl Med.* 2004;45:101–107.
34. Flier JS, Mueckler MM, Usher P, Lodish HF. Elevated levels of glucose transport and transporter messenger RNA are induced by *ras* or *src* oncogenes. *Science.* 1987;235:1492–1495.
35. Birnbaum MJ, Haspel HC, Rosen OM. Transformation of rat fibroblasts by FSV rapidly increases glucose transporter gene transcription. *Science.* 1987;235:1495–1498.
36. Smith TA. Mammalian hexokinases and their abnormal expression in cancer. *Br J Biomed Sci.* 2000;57:170–178.
37. Bell HS, Whittle IR, Walker M, Leaver HA, Wharton SB. The development of necrosis and apoptosis in glioma: experimental findings using spheroid culture systems. *Neuropathol Appl Neurobiol.* 2001;27:291–304.
38. Bos R, van Der Hoeven JJ, van Der Wall E, et al. Biologic correlates of ^{18}fluorodeoxyglucose uptake in human breast cancer measured by positron emission tomography. *J Clin Oncol.* 2002;20:379–387.
39. Oshida M, Uno K, Suzuki M, et al. Predicting the prognoses of breast carcinoma patients with positron emission tomography using 2-deoxy-2-fluoro[^{18}F]-D-glucose. *Cancer.* 1998;82:2227–2234.
40. Lucignani G, Jereczek-Fossa BA, Orecchia R. The role of molecular imaging in precision radiation therapy for target definition, treatment planning optimisation and quality control. *Eur J Nucl Med Mol Imaging.* 2004;31:1059–1063.